Journal of ELECTRONIC MATERIALS, Vol. 41, No. 9, 2012
DOI: 10.1007/s11664-012-2159-6

Thermoelectric and Magnetic Properties of $Ca_{0.98}RE_{0.02}MnO_{3-\delta}$ (RE = Sm, Gd, and Dy)

ANKAM BHASKAR,[1] CHIA-JYI LIU,[1,2] and J.J. YUAN[1]

1.—Department of Physics, National Changhua University of Education, Changhua 500, Taiwan.
2.—e-mail: liucj@cc.ncue.edu.tw

Polycrystalline samples of $Ca_{0.98}RE_{0.02}MnO_{3-\delta}$ (RE = Sm, Gd, and Dy) have been prepared by conventional solid-state reactions and their properties measured at 300 K to 700 K. All samples were single phase with orthorhombic structure. The average valence and oxygen content of $Ca_{0.98}RE_{0.02}MnO_{3-\delta}$ were determined by iodometric titration. Doping at the Ca site by rare-earth metals causes a strong decrease of electrical resistivity due to the creation of charge carrier content by Mn^{3+} in the Mn^{4+} matrix, as evidenced by iodometric titration results. The Seebeck coefficient of all the samples was negative, indicating that the predominant carriers are electrons over the entire temperature range. Among the doped samples, $Ca_{0.98}Dy_{0.02}MnO_{3-\delta}$ had the highest dimensionless figure of merit of 0.073 at 612 K, representing an improvement of about 115% with respect to the undoped $CaMnO_{3-\delta}$ sample at the same temperature. All the samples exhibited an antiferromagnetic transition with Néel temperature of around 120 K. Magnetization measurements indicated that $Ca_{0.98}RE_{0.02}MnO_{3-\delta}$ samples exhibited a high-spin state of Mn^{3+}.

Key words: Oxides, sintering, thermoelectric, thermal conductivity, magnetic properties

INTRODUCTION

Thermoelectric energy conversion can be used to generate electricity from waste heat. The efficiency of thermoelectric materials in this process is determined by their dimensionless thermoelectric figure of merit, $ZT = S^2\sigma T/\kappa$, where S, σ, T, and κ are the Seebeck coefficient, electrical conductivity, absolute temperature, and thermal conductivity, respectively.[1,2] In the past few decades, several innovative bulk intermetallic compounds that exhibit high values of ZT ($\sim$1) have been identified and developed.[3–5] Despite their high ZT values, these compounds are of limited practical use because of their low chemical stability in air at high temperatures. Realization of widespread, large-scale industrial use of thermoelectric technology is contingent on the development of low-cost thermoelectric bulk materials that are environmentally friendly and stable at high temperatures in air. Thermoelectric bulk oxides have attracted considerable attention because they fulfill these requirements. Since the discovery of p-type Na_xCoO_2,[6] which has an unexpectedly high absolute value of S despite possessing metallic conductivity, several researchers have made extensive studies on oxide materials; For instance, the p-type misfit-layered cobaltites $Ca_3Co_4O_{9+\delta}$ and $Bi_2Sr_2Co_2O_9$ have been shown to exhibit high ZT values at high temperatures in air.[7,8] Compared with the p-type oxide thermoelectric materials, there are relatively few n-type oxide materials. Among the n-type oxide materials, $CaMnO_{3-\delta}$ is the most promising. $CaMnO_{3-\delta}$ has attracted attention as a potential n-type oxide thermoelectric material for use in thermoelectric generators. Ohtaki et al.[9] and Funahashi et al.[10] studied the thermoelectric properties of $CaMnO_{3-\delta}$ by substituting Bi, Y, La, Ce, and rare-earth metals such as Nd, Tb, Ho, Yb, and Lu at the Ca site. They reported that the electrical conductivity increased considerably, while the Seebeck coefficient decreased slightly. It was also found that, when substituting Pr, Sr, and Mo at the Ca site of $CaMnO_{3-\delta}$, the thermoelectric properties

(Received March 1, 2012; accepted May 26, 2012; published online June 23, 2012)

improved.[11–13] Many groups have attempted to prepare $Ca_{1-x}RE_xMnO_3$ systems with higher concentration ($x \geq 0.1$) of rare-earth elements, reporting remarkable changes in thermoelectric properties.[14–16] Lemonnier et al.[17] reported that small concentration of rare-earth dopants in layered $Ca_{3.95}RE_{0.05}Mn_3O_{10}$ compounds led to a significant modification of the thermoelectric properties. According to the calculations using dynamic mean field theory in Ref. 18, it seems that the optimized *ZT* should occur at low doping level. Therefore, it is interesting to investigate the effects of small concentration of dopants on thermal and magnetic properties. Herein, we report thermoelectric and magnetic properties of $Ca_{0.98}RE_{0.02}MnO_{3-\delta}$ where RE = Sm, Gd, and Dy.

EXPERIMENTAL PROCEDURES

Polycrystalline samples of $Ca_{0.98}RE_{0.02}MnO_{3-\delta}$ (RE = Sm, Gd, and Dy) and $CaMnO_{3-\delta}$ were synthesized by solid-state reaction from $CaCO_3$, Mn_2O_3, Sm_2O_3, Gd_2O_3, and Dy_2O_3 powders. The powders were heated at 900°C for 10 h and at 1200°C for 20 h in air with intermediate grinding. The resulting powders were then pressed into parallelepipeds and sintered in air at 1200°C for 20 h. The phase purity of the resulting powders was examined using a Shimadzu XRD-6000 powder x-ray diffractometer using Fe K_α radiation. Electrical resistance measurements were carried out using standard four-probe technique. Thermopower measurements were performed between 300 K and 700 K using a steady-state technique with a temperature difference of 0.5 K to 2 K across the sample. A type E differential thermocouple was used to measure the temperature difference between the hot and cold ends of the sample, which was measured using a Keithley 2000 multimeter.[19] The temperature difference was typically between 0.5 K and 1 K. The thermopower of the sample was obtained by subtracting the thermopower of the Cu Seebeck probes. Thermal conductivity measurements were carried out using transient plane source techniques with very small temperature perturbations of the sample material using a Hot Disk thermal constants analyzer. The transient plane source technique makes use of a thin sensor element in the shape of a double spiral. The Hot Disk sensor acts as both a heat source for generating a temperature gradient in the sample and a resistance thermometer for recording the time-dependent temperature increase. The encapsulated sensor was sandwiched between two pieces of samples. During a preset time, 200 resistance recordings were taken, and from these a relation between temperature and time was established. A commercial superconducting quantum interference device magnetometer (Quantum Design) was used to characterize the magnetic properties of the samples. The oxygen content and manganese valence state were determined using iodometric titration.[20]

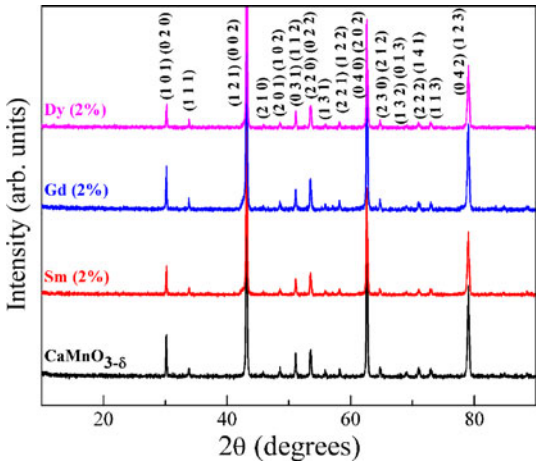

Fig. 1. XRD patterns of $CaMnO_{3-\delta}$ and $Ca_{0.98}RE_{0.02}MnO_{3-\delta}$ (RE = Sm, Gd, and Dy) (Color online).

Table I. Lattice parameters of $Ca_{0.98}RE_{0.02}MnO_{3-\delta}$ (RE = Sm, Gd, and Dy)

RE	*a* (Å)	*b* (Å)	*c* (Å)
$CaMnO_{3-\delta}$	5.27 (9)	7.43 (2)	5.26 (1)
Sm	5.25 (3)	7.42 (2)	5.27 (3)
Gd	5.24 (6)	7.43 (4)	5.28 (6)
Dy	5.27 (2)	7.42 (4)	5.25 (3)

RESULTS AND DISCUSSION

Figure 1 shows x-ray diffraction (XRD) patterns at room temperature of the $CaMnO_{3-\delta}$ and $Ca_{0.98}RE_{0.02}MnO_{3-\delta}$ (RE = Sm, Gd, and Dy) samples. All the diffraction peaks for the series of samples can be indexed based on an orthorhombic $CaMnO_{3-\delta}$ structure[21] without any measurable impurity phases, indicating that a single phase of orthorhombic $Ca_{0.98}RE_{0.02}MnO_{3-\delta}$ (RE = Sm, Gd, and Dy) is obtained for each sample. Lattice parameters were calculated and are tabulated in Table I. As seen in Table I, the lattice parameters do not show a monotonic trend, which may be due to oxygen deficiency and small amount of dopants.

Table II summarizes the characterization and properties for the series of samples at room temperature. The undoped sample shows the highest resistivity among the samples. The resistivity of the undoped sample is 0.1 Ω-cm at 300 K. The size of ρ for all doped samples is in the range 0.02 Ω-cm to 0.04 Ω-cm, decreasing with decreasing RE^{3+} ionic radius. Doping at the Ca site by rare-earth metals causes a strong decrease of ρ due to the creation of charge carrier content by Mn^{3+} in the Mn^{4+} matrix. The concentration of carriers in these samples can be correlated with the oxidation state of Mn. Creation of Mn^{3+} comes from two sources in the title system, i.e., doping of RE^{3+} (trivalent rare-earth ion) and oxygen deficiency. In other words, at the same doping level of RE^{3+}, the oxygen deficiency plays a role in the

Table II. Characterization and properties of $Ca_{0.98}RE_{0.02}MnO_{3-\delta}$ (RE = Sm, Gd, and Dy) at room temperature

RE	Mn^{V+}	δ	ρ (mΩ-cm)	S (μV/K)	κ_{total} (W/mK)	κ_{el} (W/mK)	κ_{ph} (W/mK)	PF (μW/cm-K^2)	ZT
$CaMnO_{3-\delta}$	3.90(8)	0.04(4)	102	−319	3.72	0.007	3.713	0.99	0.008
Sm	3.94(4)	0.01(2)	41	−212	2.71	0.018	2.692	1.09	0.018
Gd	3.92(8)	0.02(4)	35	−223	2.71	0.020	2.690	1.21	0.018
Dy	3.91(9)	0.03(4)	22	−175	2.86	0.034	2.826	1.41	0.020

creation of charge carriers by Mn^{3+}. The oxygen deficiency in $CaMnO_{3-\delta}$ creates two Mn^{3+} five-coordinated sites for each O vacancy according to the x-ray absorption near-edge spectra results.[22] To compensate the oxygen deficiency and maintain electrical neutrality, an excess of Mn^{3+} should therefore be present in these samples. There are also earlier reports on oxygen deficiency for other electron-doped calcium manganites.[23,24] The negative thermopower confirms that the dominant charge carriers are electrons for all the samples. The undoped $CaMnO_{3-\delta}$ has a very large absolute S, being about -319 μV K^{-1} at 300 K. The room-temperature value of absolute S for the undoped sample is lower than the value of -600 μV/K reported by Flahaut et al.[14] Our 2% doped samples exhibit higher resistivity than the values (5 mΩ-cm to ~7 mΩ-cm) for Wang's samples with 10% doping content at room temperature. Furthermore, our 2% doped samples exhibit larger thermopower than the values (-95 μV/K to -80 μV/K) for Wang's samples with 10% higher doping content at room temperature.[15] These differences can probably be attributed to the oxygen deficiency and composition variation.

The doped samples show relatively small absolute S due to the increase of carrier concentration (Table II). The rare-earth doping induces a clear decrease of the absolute S value due to the increase of the concentration of Mn^{3+}. The temperature dependences of the resistivity (ρ) and thermopower (S) of these samples were reported recently.[25] The main features of our results are: (1) Electrical resistivity for $CaMnO_{3-\delta}$ decreases with increasing temperature, a typical characteristic of nonmetal-like temperature dependence (Fig. 2a). On the other hand, the absolute value of the thermopower increases with increasing temperature, a characteristic of metal-like temperature dependence (Fig. 2b); (2) Both electrical resistivity and the absolute value of the thermopower for all doped samples $Ca_{0.98}RE_{0.02}MnO_{3-\delta}$ increase with increasing temperature, a typical characteristic of metal-like temperature dependence; (3) Both resistivity and the absolute value of the thermopower for all the doped samples show significant decreases as compared with $CaMnO_{3-\delta}$; (4) Both electrical resistivity and the absolute value of the thermopower for $CaMnO_{3-\delta}$ show significant decreases as compared with those reported by Ohtaki et al.[9] In sharp contrast to our $CaMnO_{3-\delta}$, the absolute value of thermopower of Ohtaki's sample decreases with increasing temperature, a typical

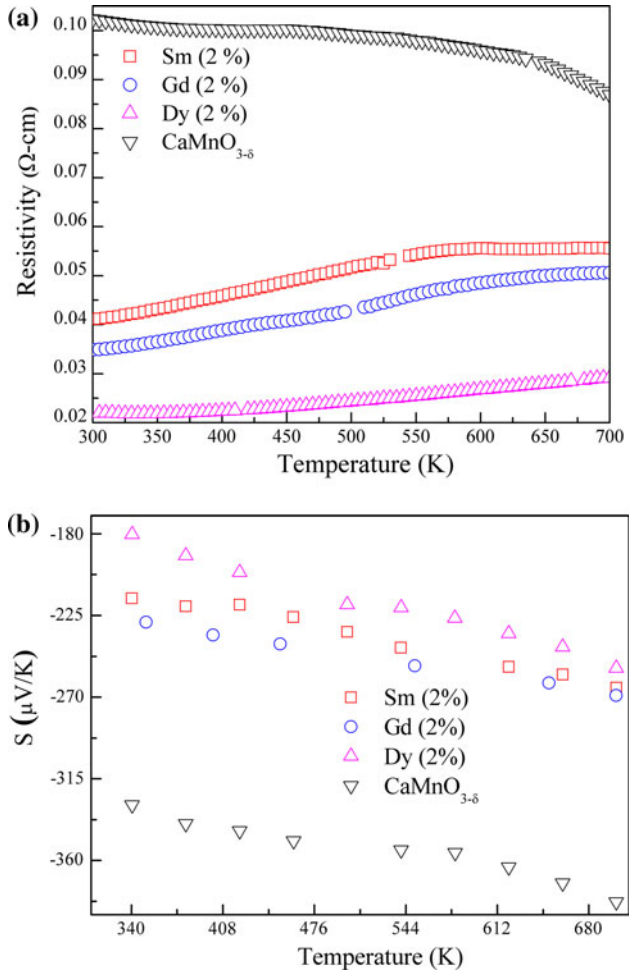

Fig. 2. (a) Temperature dependence of electrical resistivity and (b) thermopower for $CaMnO_{3-\delta}$ and $Ca_{0.98}RE_{0.02}MnO_3$ (RE = Sm, Gd, and Dy) (Color online).

characteristic of nonmetal-like temperature dependence. This difference should be attributed to the contribution of the oxygen deficiency.[25]

The temperature dependence of the power factor (PF) ($S^2\sigma$) is shown in Fig. 3. It can be seen that the values of power factor for all the samples increase with increasing temperature. The highest value of $S^2\sigma$ = 2.21 μW cm^{-1} K^{-2} at 700 K is obtained for $Ca_{0.98}Dy_{0.02}MnO_{3-\delta}$ as a result of its low ρ value combined with its moderate absolute S value. Muguerra et al.[26] reported a power factor of ~2.1 μW cm^{-1} K^{-2} at 700 K for $Ca_{0.98}Dy_{0.02}MnO_3$, which is lower than for our sample. $Ca_{0.98}Dy_{0.02}MnO_{3-\delta}$ exhibits a higher

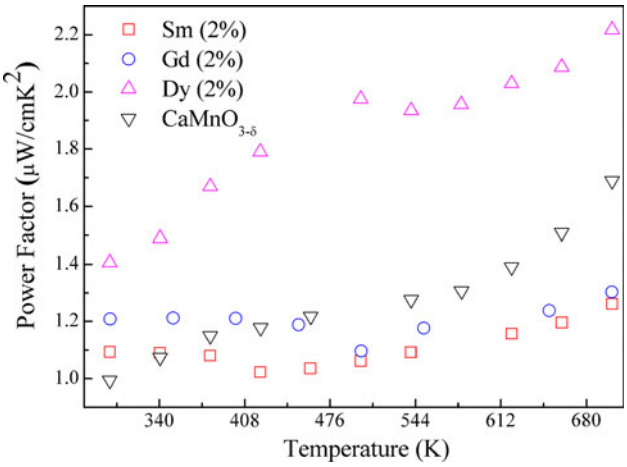

Fig. 3. The temperature dependence of the power factor of $CaMnO_{3-\delta}$ and $Ca_{0.98}RE_{0.02}MnO_{3-\delta}$ (RE = Sm, Gd, and Dy) (Color online).

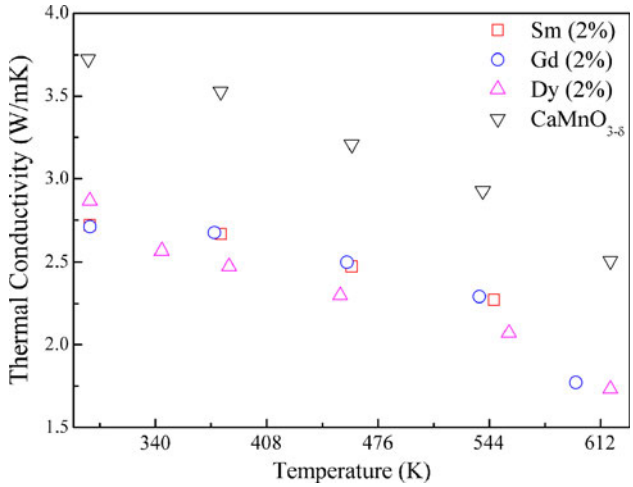

Fig. 4. The temperature dependence of the thermal conductivity κ of $CaMnO_{3-\delta}$ and $Ca_{0.98}RE_{0.02}MnO_{3-\delta}$ (RE = Sm, Gd, and Dy) (Color online).

power factor of 2.21 μW cm^{-1} K^{-2} at 700 K than that reported by Park et al.[27] because our sample shows a lower ρ value of 2.9 mΩ-cm and higher S value of -254 μV/K. Park et al.[27] reported that the highest power factor of 0.37 μW cm^{-1} K^{-2} occurred at 800 K for $Ca_{0.8}Dy_{0.2}MnO_3$ with ρ = 8.3 mΩ-cm and S = -55 μV/K.

The temperature dependence of the thermal conductivity is shown in Fig. 4. To examine the values of thermal conductivity for our samples in more detail, the lattice contribution κ_{ph} was estimated by the equation below. The total thermal conductivity κ_{total} of solids can be written as

$$\kappa_{total} = \kappa_{el} + \kappa_{ph}, \quad (1)$$

where κ_{el} and κ_{ph} represent the electronic and lattice thermal conductivity, respectively. κ_{el} can be calculated by using the Wiedemann–Franz relationship,

$$\kappa_{el} = L\sigma T, \quad (2)$$

where $L = \pi^2k^2/3e^2 = 2.45 \times 10^{-8}$ W Ω K^{-2} is the Lorenz number, σ is the electrical conductivity, and T is the absolute temperature. κ_{ph} is obtained by subtracting κ_{el} from κ_{total}. The undoped sample has κ_{total} = 3.4 W m^{-1} K^{-1}, which is similar to the value κ_{total} = 3.6 W m^{-1} K^{-1} at room temperature reported by Flahaut et al.[14] It can be clearly seen from Table II that the total thermal conductivity for all the doped samples is less than that of $CaMnO_{3-\delta}$. For materials with $\rho > 1$ Ω-cm, κ_{el} is negligible. However, in our case, the resistivity is lower than 1 Ω-cm, a fact which leads us to determine κ_{el} by using the Wiedemann–Franz law. The calculated value of κ_{el} for $CaMnO_{3-\delta}$ is 0.019 W m^{-1} K^{-1}, and that for $Ca_{0.98}Dy_{0.02}MnO_{3-\delta}$ is 0.059 W m^{-1} K^{-1}, at 700 K. For all the samples, the lattice contribution is more important than the electronic one. Due to the small κ_{el}, κ_{total} is mainly attributed to the lattice contribution. As reported by Cong et al.,[11] rare-earth metal substitution induces a decrease of κ_{ph} due to the phonon–lattice defect interaction. Moreover, for the same RE^{3+} content, the size of κ_{total} increases from Sm to Dy substitution. Both κ_{el} and κ_{ph} decrease with decreasing RE^{3+} ionic radius (Table II). The effect of RE^{3+} doping on the lattice vibration arises from two main factors. One is the crystallographic distortion caused by the change in ionic radius. The other factor is that the weight of RE^{3+} is much higher than Ca^{2+}. Flahaut et al.[14] also reported that in this system κ strongly depends on the atomic weight at the A site but to a lesser extent on the ionic radius. Due to the large difference of weight between RE^{3+} and Ca^{2+}, the RE^{3+} ions can vibrate independently from the other ions, which can cause large local vibrations.[15] As a result, the mean free path of phonons will be shortened, and thus κ_{ph} will be markedly suppressed. At the same time, the mass difference between RE^{3+} and Ca^{2+} will cause further reduction in κ_{ph}.

Based on the data of $\rho(T)$, $S(T)$, and $\kappa(T)$, the dimensionless figure of merit $ZT = S^2\sigma T/\kappa$ was calculated for all the samples. The obtained results are shown in Fig. 5. The ZT values for all the samples increase with increasing temperature over the entire temperature range. The highest ZT is obtained for $Ca_{0.98}Dy_{0.02}MnO_{3-\delta}$, because of its low values of ρ and κ, and moderate value of S. The doped samples exhibit higher ZT values than $CaMnO_{3-\delta}$ because of the reduction of ρ and κ. We obtain ZT = 0.073 at 612 K for $Ca_{0.98}Dy_{0.02}MnO_{3-\delta}$, which represents a 115% increase when compared with $CaMnO_{3-\delta}$. $Ca_{0.98}Dy_{0.02}MnO_{3-\delta}$ exhibited a higher value of ZT = 0.073 than reported by Wang et al.[28] and Kosuga et al.[29] at the same temperature. Wang et al.[28] reported ZT values of 0.035, 0.058, and 0.060 at 600 K for $Ca_{0.95}Ce_{0.05}MnO_3$, $Ca_{0.9}Y_{0.1}MnO_3$, and $Ca_{0.9}La_{0.1}MnO_3$, respectively. Kosuga et al.[29]

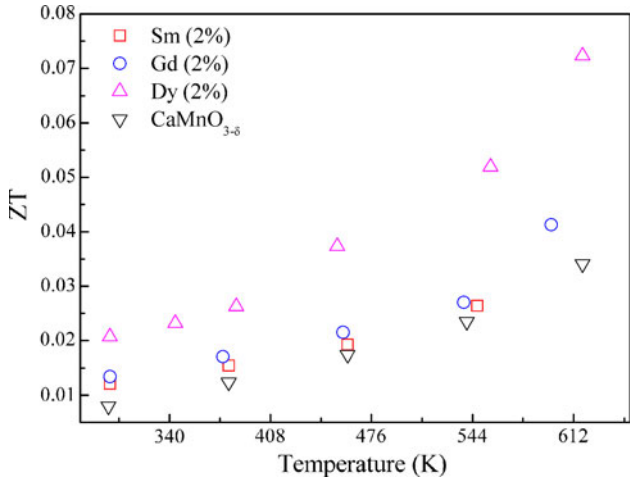

Fig. 5. The temperature dependence of the dimensionless figure of merit ZT of $CaMnO_{3-\delta}$ and $Ca_{0.98}RE_{0.02}MnO_{3-\delta}$ (RE = Sm, Gd, and Dy) (Color online).

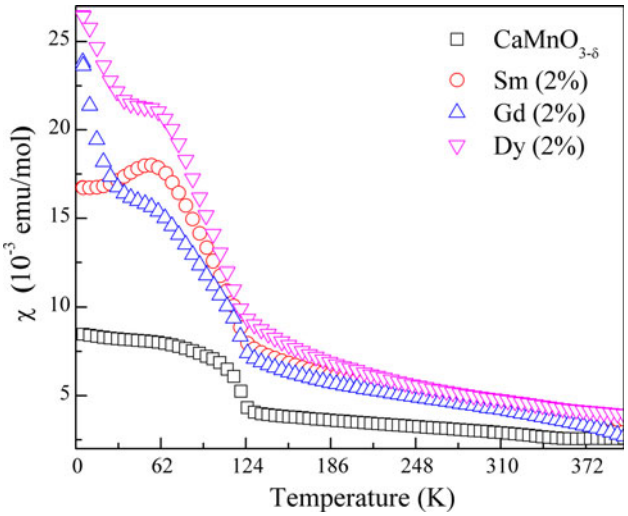

Fig. 6. The temperature dependence of the magnetic susceptibility for $CaMnO_{3-\delta}$ and $Ca_{0.98}RE_{0.02}MnO_{3-\delta}$ (RE = Sm, Gd, and Dy) in applied field of 50,000 Oe (Color online).

reported a ZT value of 0.05 at 600 K for $Ca_{0.7}Sr_{0.2}Yb_{0.1}MnO_{3-\delta}$. Muguerra et al.[26] reported a ZT value of ~0.019 at 300 K for the $Ca_{0.98}Dy_{0.02}MnO_3$ system, which is in agreement with our value for $Ca_{0.98}Dy_{0.02}MnO_{3-\delta}$ of ZT = 0.020 at 300 K. These results suggest that there is scope for improving ZT of n-type $CaMnO_{3-\delta}$ for high-temperature thermoelectric applications.

Figure 6 shows the magnetic susceptibility (χ) as a function of temperature for $CaMnO_{3-\delta}$ and $Ca_{0.98}RE_{0.02}MnO_{3-\delta}$ (RE = Sm, Gd, and Dy). The $Ca_{0.98}RE_{0.02}MnO_{3-\delta}$ samples differ from that of $CaMnO_{3-\delta}$ by the appearance of a small kink at around T = 65 K, which may be due to a cluster-glass state.[30] The RE^{3+} ions replace Ca^{2+} at the A site, but their fraction is too low to establish long-range magnetic order. Instead of this, due to Mn^{3+}–Mn^{4+} exchange interactions, short-range ordering occurs, forming ferromagnetic clusters in the antiferromagnetic matrix. Maignan et al.[30] reported that the cluster-glass state (T_{CG}) was observed at T_m = 68 K for the $Ca_{0.975}Sm_{0.025}MnO_3$ system. Hejtmanek et al.[31] also reported that T_{CG} was observed at 110 K for $Ca_{0.95}Sm_{0.05}MnO_3$. However, more work is necessary to elucidate further details of the cluster-glass state at low temperatures. The Néel transition temperatures (T_N) were obtained from the inflection point of the $d\chi/dT$ versus temperature curves and are given in Table III. It is clear from the table that the T_N values lie in the range from 115 K to 120 K for all the samples. Moritomo et al.[32] reported that the antiferromagnetic transition for $CaMnO_{3-\delta}$ occurred at T_N = 120 K, which is in agreement with our undoped sample result (T_N). The magnetic susceptibility in the paramagnetic region can be described by the Curie–Weiss law, i.e., $\chi = C/(T + \theta_p)$, where C is the Curie–Weiss coefficient, being related to the effective magnetic moment μ_{eff}; θ_p is the paramagnetic Curie–Weiss temperature. Table III presents the calculated values of μ_{eff}, C, and θ_p for the $CaMnO_{3-\delta}$ and $Ca_{0.98}RE_{0.02}MnO_{3-\delta}$ (RE = Sm, Gd and Dy) samples from the best fits (above 150 K). The Curie–Weiss temperature (θ_p) is related to the strength of the antiferromagnetic interaction. θ_p is large and negative for $CaMnO_{3-\delta}$, indicating antiferromagnetic interaction. A few researchers have previously reported[22,33] that the magnitude of θ_p is high, which can be explained by the G-type antiferromagnetic interaction.

The observed effective magnetic moments lie between 4.23 and 4.07 μ_B (Table III). The observed effective magnetic moment of $CaMnO_{3-\delta}$ (μ_{eff} = 4.15 μ_B) is lower than the reported value ($\mu_{eff} \approx 4.37\ \mu_B$), which may be due to the absence of spin-glass behavior.[22] Wiebe et al.[34] reported that differences between the experimental and calculated effective magnetic moments have been attributed to ferromagnetic interactions from Mn^{3+}–Mn^{4+} clusters. Nakade et al.[35] reported that the observed effective magnetic moment of $CaMnO_{3-\delta}$ was 3.69μ_B, which was due to the low-spin state of the Mn^{3+} ion. To the best of our knowledge, there is only one previous report in the literature regarding the extraction of the effective magnetic moment value from the Curie–Weiss law for higher concentration (0.1) of rare-earth-doped $CaMnO_3$.[36] The theoretical effective magnetic moment is calculated by

$$\mu_{eff} = \sqrt{0.98\mu^2_{eff,Mn^{4+}} + 0.02\mu^2_{eff,Mn^{3+}} + 0.02\mu^2_{eff,RE^{3+}}}. \quad (3)$$

The effective magnetic moments of Sm^{3+}, Gd^{3+}, and Dy^{3+} are 0.85 μ_B/f.u., 7.9 μ_B/f.u., and 10.6 μ_B/f.u., respectively. According to the energy band scheme for perovskite manganites,[37] the electron configuration of Mn^{4+} and Mn^{3+} ions are $3d^3$ and $3d^4$, respectively. With respect to the crystal-field splitting between the t_{2g} and e_g states and the Hund coupling energy (exchange energy), the spin state configuration of

Table III. Magnetic properties of $Ca_{0.98}RE_{0.02}MnO_{3-\delta}$ (RE = Sm, Gd, and Dy)

RE	T_N (K)	C (emu K/mol)	θ_p (K)	μ_{eff} (μ_B)
$CaMnO_{3-\delta}$	120	2.15	−408	4.15
Sm	115	2.53	−224	4.50
Gd	120	2.20	−198	4.20
Dy	115	2.21	−162	4.21

Mn^{4+} is $t_{2g}^3e_g^0$, yielding a total spin $S = 3/2$ with effective magnetic moment $3.9\mu_B$, whereas the Mn^{3+} can exist either in the high-spin (HS) state $t_{2g}^3e_g^1$ yielding total spin $S = 2$ with effective magnetic moment $4.9\mu_B$, or the low-spin (LS) state $t_{2g}^4e_g^0$ yielding total spin $S = 1$ with effective magnetic moment $2.8\mu_B$. The calculated effective magnetic moments of $Ca_{0.98}RE_{0.02}MnO_3$ are $3.88\mu_B$ (Mn^{3+} LS) and $3.92\mu_B$ (Mn^{3+} HS) for RE = Sm, $4.04\mu_B$ (Mn^{3+} LS) and $4.07\mu_B$ (Mn^{3+} HS) for RE = Gd, and $4.16\mu_B$ (Mn^{3+} LS) and $4.19\mu_B$ (Mn^{3+} HS) for RE = Dy, respectively. It can be seen from the table that the $Ca_{0.98}RE_{0.02}MnO_{3-\delta}$ (RE = Sm, Gd, and Gd) system has high-spin state of Mn^{3+}, which supports the transport properties of $Ca_{0.98}RE_{0.02}MnO_{3-\delta}$ (RE = Sm, Gd, and Gd).[25] Both the substitution of a trivalent rare-earth cation for divalent Ca and the presence of the oxygen defect induce partial occupation of e_g states. The hybridization between Mn 3d e_g and O 2p orbitals could develop an impurity band for the title system in a similar way as for degenerate semiconductors.[25] Wang et al.[36] reported that the HS state of Mn^{3+} was observed below the metal–insulator transition temperature (T_{MI}) and partial Mn^{3+} ions changed from the HS to the LS state above T_{MI} in $Ca_{0.9}RE_{0.1}MnO_3$ (RE = La, Pr, and Yb). In addition, the transition temperatures (T_{MI}) were observed in the range from 325 K to 420 K. Our results do not exhibit any MI transition in this temperature range, which may be due to the oxygen deficiency and composition variation. It should be noted that the partial unoccupied O 2p states could contribute to the magnetic moments.[38] The presence of Mn^{3+} of high spin state could enhance the hybridization between Mn 3d and O 2p.

CONCLUSIONS

The effects of rare-earth element doping at the Ca site on the thermoelectric properties of $Ca_{0.98}RE_{0.02}MnO_{3-\delta}$ (RE = Sm, Gd, and Dy) have been investigated in an attempt to improve the thermoelectric performance of the materials. All samples were single phase with orthorhombic structure. The rare-earth dopant elements had remarkable effects on the transport behavior of the title system. The highest ZT was reached for $Ca_{0.98}Dy_{0.02}MnO_{3-\delta}$, being 115% higher than that of undoped $CaMnO_{3-\delta}$. These results suggest that 2% doping of rare-earth metals at the calcium site of the $CaMnO_{3-\delta}$ phase results in reduction of resistivity and thermal conductivity. The effective magnetic moment was determined from the temperature dependence of the paramagnetic susceptibility.

ACKNOWLEDGEMENTS

This work was supported by the National Science Council of Taiwan, R.O.C. under Grant No. NSC 98-2112-M-018-005-MY3. A.B. would like to acknowledge a postdoctoral fellowship sponsored by the National Science Council of Taiwan.

REFERENCES

1. D.G. Mahan, *Solid State Phys.* 51, 81 (1998).
2. T.M. Tritt, *Science* 283, 804 (1999).
3. B.C. Sales, D. Mandrus, and R.K. Williams, *Science* 272, 1325 (1996).
4. D.-Y. Chung, T. Hogan, P. Brazis, M.R. Lane, C. Kamewurf, M. Bastea, C. Uher, and M.G. Kanatzidis, *Science* 287, 1024 (2000).
5. T. Caillat, J.-P. Fleurial, and A. Borshchevsky, *J. Phys. Chem. Solids* 58, 1119 (1997).
6. I. Terasaki, Y. Sasago, and K. Uchinokura, *Phys. Rev. B* 56, R12685 (1997).
7. C.-J. Liu, L.-C. Huang, and J.-S. Wang, *Appl. Phys. Lett.* 89, 204102 (2006).
8. R. Funahashi and I. Matsubara, *Appl. Phys. Lett.* 79, 362 (2001).
9. M. Ohtaki, H. Koga, T. Tokunaga, K. Eguchi, and H. Arai, *J. Solid State Chem.* 120, 105 (1995).
10. R. Funahashi, A. Kosuga, N. Miyasou, E. Takeuchi, S. Urata, K. Lee, H. Ohta, and K. Koumoto, *Proceeding of the 26th International Conference on Thermoelectrics* (ICT-2007), South Korea, pp. 124–128.
11. B.T. Cong, T. Tsuji, P.X. Thao, P.Q. Thanh, and Y. Yamamura, *Phys. B* 352, 18 (2004).
12. G. Xu, R. Funahashi, I. Matsubara, M. Shiano, and Y. Zhou, *J. Mater. Res.* 17, 1092 (2002).
13. M. Miclau, S. Herbert, R. Retoux, and C. Martin, *J. Solid State Chem.* 178, 1104 (2005).
14. D. Flahaut, T. Mihara, R. Funahashi, N. Nabeshima, K. Lee, H. Ohta, and K. Koumoto, *J. Appl. Phys.* 100, 084911 (2006).
15. Y. Wang, Y. Sui, and W. Su, *J. Appl. Phys.* 104, 093703 (2008).
16. S.-M. Choi, C.-H. Lim, and W.-S. Seo, *J. Electron. Mater.* 40, 551 (2011).
17. S. Lemonnier, E. Guilmeau, C. Goupil, R. Funahashi, and J.G. Noudem, *Ceram. Int.* 36, 887 (2010).
18. Y. Wang, Y. Sui, H. Fan, X. Wang, Y. Su, W. Su, and X. Liu, *Chem. Mater.* 21, 4653 (2009).
19. C.-J. Liu, *Philos. Mag. B* 79, 1145 (1999).
20. C.-J. Liu, M.D. Mays, D.O. Cowan, and M.G. Sánchez, *Chem. Mater.* 3, 495 (1991).
21. K.R. Poeppelmeier, M.E. Leonowicz, J.C. Scanlon, J.M. Longo, and W.B. Yelon, *J. Solid State Chem.* 45, 71 (1982).
22. Z. Zeng, M. Greeblatt, and M. Croft, *Phys. Rev. B* 59, 8784 (1999).
23. H. Taguchi and M. Shimada, *J. Solid State Chem.* 63, 290 (1986).
24. H. Taguchi, M. Nagao, and M. Shimada, *J. Solid State Chem.* 82, 8 (1989).
25. C.-J. Liu, A. Bhaskar, and J.J. Yuan, *Appl. Phys. Lett.* 98, 214101 (2011).
26. H. Muguerra, B.R. Murias, M. Traianidis, C. Marchal, P. Vanderbemden, B. Vertruyen, C. Henrist, and R. Cloots, *J. Alloys Compd.* 509, 7710 (2011).
27. K. Park and G.W. Lee, *Nanoscale Res. Lett.* 6, 548 (2011).
28. Y. Wang, Y. Sui, X. Wang, and W. Su, *J. Phys. D Appl. Phys.* 42, 055010 (2009).
29. A. Kosuga, Y. Isse, Y. Wang, K. Koumoto, and R. Funahashi, *J. Appl. Phys.* 105, 093717 (2009).
30. A. Maignan, C. Martin, F. Damay, B. Raveau, and J. Hejtmanek, *Phys. Rev. B* 58, 2758 (1998).

31. J. Hejtmanek, Z. Jirak, M. Marysko, C. Martin, A. Maignan, M. Hervieu, and B. Raveau, *Phys. Rev. B* 60, 14057 (1999).
32. Y. Moritomo, A. Machida, E. Nishibori, M. Takata, and M. Sakata, *Phys. Rev. B* 64, 214409 (2001).
33. I.D. Fawcett, J.E. Sunstrom IV, M. Greenblatt, M. Croft, and K.V. Ramanujachary, *Chem. Mater.* 10, 3643 (1998).
34. C.R. Wiebe, J.E. Greedan, J.S. Garden, Z. Zeng, and M. Greenblatt, *Phys. Rev. B* 64, 064421 (2001).
35. K. Nakade, K. Hirota, M. Kato, and H. Taguchi, *Mater. Res. Bull.* 42, 1069 (2007).
36. Y. Wang, Y. Sui, J. Cheng, X. Wang, Z. Lu, and W. Su, *J. Phys. Chem. C* 113, 12509 (2009).
37. J.B. Goodenough, *J. Appl. Phys.* 37, 1415 (1966).
38. J.L. Chen, Y.S. Liu, C.-J. Liu, L.-C. Huang, C.L. Dong, S.S. Chen, and C.L. Chang, *J. Phys. D Appl. Phys.* 42, 135418 (2009).